Representing the impact of *Rhizophora* mangroves on flow in a hydrodynamic model (COAWST_rh v1.0): the importance of three-dimensional root system structures

Masaya Yoshikai[1,2], Takashi Nakamura[1], Eugene C. Herrera[3], Rempei Suwa[4], Rene Rollon[5], Raghab Ray[6], Keita Furukawa[7], and Kazuo Nadaoka[1]

[1]School of Environment and Society, Tokyo Institute of Technology, Tokyo 152-8552, Japan
[2]Coastal Marine Group, School of Science, University of Waikato, Private Bag 3105, Hamilton, 3240, New Zealand
[3]Institute of Civil Engineering, University of the Philippines, Diliman, Quezon City 1101, Philippines
[4]Forestry Division, Japan International Research Center for Agricultural Sciences (JIRCAS), Ibaraki 305-8686, Japan
[5]Institute of Environmental Science & Meteorology, College of Science, University of the Philippines, Diliman, Quezon City, 1001, Philippines
[6]Atmosphere and Ocean Research Institute, The University of Tokyo, Chiba, 277-8564, Japan
[7]NPO Association for Shore Environment Creation, Kanagawa, 220-0023, Japan

Correspondence to: Masaya Yoshikai (yoshikai.masaya@gmail.com)

Abstract. Coastal wetland vegetations modulate water flow by exerting drag which has an important implication on sediment transport and geomorphic dynamics. This vegetation effect on flow is commonly represented in hydrodynamic models by approximating the vegetations as an array of vertical cylinders or increased bed roughness. However, this simple approximation may not be valid in the case of *Rhizophora* mangroves that have complicated three-dimensional root structures. Here, we present a new model to represent the impacts of *Rhizophora* mangroves on flow in hydrodynamic models. The model explicitly accounts for the effects of the three-dimensional root structures on mean flow and turbulence, as well as the effects of two different length scales of vegetation-generated turbulence characterized by stem diameter and root diameter. The model employs an empirical model for the *Rhizophora* root structures that can be applied using basic vegetation parameters (mean stem diameter and tree density) without rigorous measurements of the root structures. We tested the model against the flows measured in a model mangrove forest in the laboratory and an actual mangrove forest in the field from previous studies. We show that compared to the conventional approximation using an array of cylinders or increased bed roughness, the new model significantly improves the predictability of velocity, turbulent kinetic energy, and bed shear stress in the *Rhizophora* mangrove forests. Overall, the presented new model offers a more realistic but feasible framework for simulating flows in *Rhizophora* mangrove forests with complex root structures using hydrodynamic models.

1 Introduction

Mangroves are one of the coastal wetland habitats that grow in intertidal areas in tropical and subtropical regions (Hamilton and Casey, 2016). They have characteristic aboveground root systems with varying morphological structures among

genera, such as pneumatophores or "pencil roots" of *Avicennia* and *Sonneratia*, and prop roots of *Rhizophora* (Krauss et al., 2014). Especially due to the presence of aboveground root systems, mangroves exert drag against water flow that lowers flow velocity. This creates conditions preferable for the deposition and retention of tidally and fluvially transported sediments (Furukawa et al., 1997; Krauss et al., 2003; Horstman et al., 2015; Chen et al., 2016, 2018; Willemsen et al., 2016; Best et al., 2022) similar to other wetland habitats such as salt marshes (Temmerman et al., 2005; Bouma et al., 2007; Mudd et al., 2010; Weisscher et al., 2022). The flow-vegetation interactions coupled with sediment transport play a major role in driving the long-term geomorphic evolution of wetland habitats (Mariotti and Fagherazzi, 2010; Mariotti and Canestrelli, 2017; Brückner et al., 2019; Kalra et al., 2022; Willemsen et al., 2022). This further determines the persistence of mangroves amidst threats due to sea-level rise (Fagherazzi et al., 2012, 2020; Lovelock et al., 2015; Kirwan et al., 2016).

Representing the effect of vegetation on flow (vegetation drag) in hydrodynamic models is important to advance our understanding of hydrodynamics in coastal wetlands with implications on sediment transport and geomorphic dynamics (Temmerman et al., 2005; Nardin et al., 2016; Lokhorst et al., 2018). Several modeling studies have shown that depending on the magnitude of vegetation drag, the resulting geomorphic evolution can vary dramatically, and correspondingly, the ecosystems' fate in response to sea-level rise (Boechat Albernaz et al., 2020; Xie et al., 2020). The vegetation drag in salt marshes and seagrass beds is commonly represented in hydrodynamic models by an array of vertical cylinders (cylinder drag model; Ashall et al., 2016; Zhu et al., 2020), the drag effect of which has been well studied both for emergent and submerged cases (e.g., Nepf, 1999, 2012). Although fewer compared to studies on salt marshes, some studies have incorporated the drag effects of mangroves in hydrodynamic models to evaluate their role in controlling flow and sediment transport (van Maanen et al., 2015; Bryan et al., 2017; Mullarney et al., 2017; Rodríguez et al., 2017; Xie et al., 2020). However, most of them are limited to *Avicennia* or *Sonneratia*-dominated mangrove forests whose aboveground roots (pencil roots) are geometrically simple and resemble that of a cylinder array.

In contrast, the root system of *Rhizophora* genus (prop root system) has three-dimensionally complicated structures that cannot simply be approximated by the array of vertical cylinders. Consequently, the representation of drag by *Rhizophora* mangroves in hydrodynamic models remains to be established despite the worldwide occurrences of this mangrove genus (Friess et al., 2019). This knowledge gap can be seen in the studies that have approximated the drag by *Rhizophora* mangroves with arbitrarily increased bed roughness (Zhang et al., 2012) or cylinder arrays with arbitrary cylinder density (Xie et al., 2020) without much theoretical and experimental support (reviewed in Le Minor et al., 2021). One exception is a modeling study by Horstman et al. (2015) that approximated the root structures of *Rhizophora* mangroves using a cylinder array with vertically variable cylinder densities. However, their method requires an exhausting field survey of the root structures as a requirement for proper model application, which may not be feasible for a forest-scale simulation.

In addition to flow velocity, vegetation affects turbulence (Nepf, 2012; Xu and Nepf, 2020), which is also relevant to the transport of substances (e.g., sediment and solutes) through turbulent diffusion (Tanino and Nepf, 2008; Xu and Nepf, 2021). While several hydrodynamic models can account for vegetation-generated turbulence (e.g., Temmerman et al., 2005, Marsooli

et al., 2016), so far, no model has been established to predict the turbulence structures in *Rhizophora* mangrove forests. A rigorous, but feasible representation of the impact of *Rhizophora* mangroves on flow velocity and turbulence in a hydrodynamic model is thus needed.

One of the challenges in modeling the flow in *Rhizophora* mangroves is the quantification of the complex root structures that can be labor-intensive when applied to a forest scale. Recently, an empirical model to predict the structures of *Rhizophora* root systems from stem diameter was proposed by Yoshikai et al. (2021). The model's general applicability to the root structures of various tree sizes has been extensively confirmed (Yoshikai et al., 2021). This empirical *Rhizophora* root model (hereafter denoted as *Rh*-root model) offers the possibility to feasibly simulate the flow in the forest scale once it is implemented in the hydrodynamic model.

In order to contribute to realistic but feasible simulations of hydrodynamics in *Rhizophora* mangrove forests, here, we implement a new drag and turbulence model coupled with the *Rh*-root model to represent the impacts of *Rhizophora* mangroves in a three-dimensional hydrodynamic model–the Regional Ocean Modeling System (ROMS; Shchepetkin and McWilliams, 2005) of the model framework COAWST (Coupled Ocean–Atmosphere–Wave–Sediment Transport Modeling System; Warner et al., 2010). The impact of the vertically varying projected area of roots on flow velocity and turbulence is specifically taken into consideration by the new model. Furthermore, the new model accounts for two different length scales of turbulence generated by *Rhizophora* mangroves–stem diameter and root diameter–as characterized by a flume experiment by Maza et al. (2017). Here, we aim to examine the following: (a) how does the consideration of the three-dimensional root structures of *Rhizophora* mangroves in the hydrodynamic model improve the predictability of flow velocity and turbulence compared to the conventional drag approximation using cylinder arrays or increased bed roughness? (b) how can the new model be effectively applied to *Rhizophora* mangrove forests in the field with limited known root parameters?

2 Materials and Methods

2.1 Model description

A proposed framework for modeling the flow in *Rhizophora* mangrove forests is presented in Fig. 1. We used a three-dimensional hydrodynamic model, ROMS, in the model framework COAWST. The vegetation module has been added by Beudin et al. (2017) to account for the drag by vegetation (such as seagrasses and salt marshes) in the momentum equations in ROMS. The equations added by Beudin et al. (2017) are basically in the same form as the cylinder drag model (see Text S1 in the Supporting Information). We modified these equations to make them suitable for representing the impact of *Rhizophora* mangroves on flow; these equations are described below (Sections 2.1.1 and 2.1.2). We added a new module in COAWST–the *Rhizophora* root module–that provides the vertical profile of the projected area density of root systems from stem diameter and tree density in each model grid (Fig. 1; Section 2.1.3).

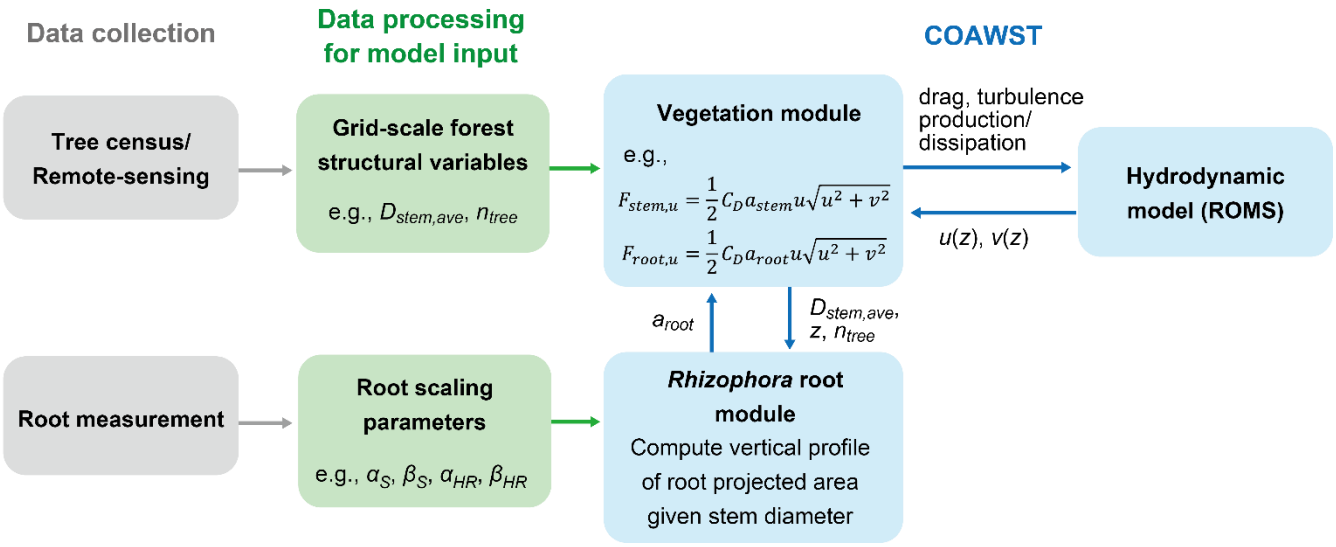

Figure 1. The proposed framework of modeling flow in *Rhizophora* mangrove forests using COAWST. $D_{stem,ave}$ and n_{tree} are the mean stem diameter and tree density, respectively, to be given in each grid, a_{stem} and a_{root} are the stem and root projected area density, where a_{stem} is a product of $D_{stem,ave}$ and n_{tree}. $F_{stem,u}$ and $F_{root,u}$ are the drag forces exerted on the *u*-component of flow by the stem and root, respectively. See Text S3 and Table S1 for explanations of the root scaling parameters.

This manuscript considers velocities as temporally averaged unless specified. We did not consider the subgrid-scale spatial heterogeneity of velocity generated by vegetation as in other modeling studies (e.g., King et al., 2012; Marsooli et al., 2016). The Reynolds number (*Re*) defined using the root diameter as length scale could be higher than the value ensuring fully turbulent structures of root-generated wakes (*Re* > 120; Shan et al., 2019) even for weak currents (~1 cm s^{-1}) that could diminish the dependence of drag coefficient (C_D) on *Re*. Thus, we treat C_D as a constant as in Beudin et al. (2017). For simplicity, we present equations in the two-dimensional form on the *x*-*z* plane (zero velocity in *y*-direction) while the equations implemented in ROMS are three-dimensional (*x*-*y*-*z*), where *x*-*y* represents the horizontal plane and *z* represents the vertical direction.

2.1.1 Drag force

In *Rhizophora* mangrove forests, the stem and roots are the main components that exert drag in tidal flows. We partition the drag by *Rhizophora* mangroves (vegetation drag) into the contributions by stems and roots and calculated it using the quadratic drag law as

$$F_{veg}(z) = F_{stem}(z) + F_{root}(z) = \frac{1}{2} C_D n_{tree} D_{stem,ave} u(z)^2 + \frac{1}{2} C_D a_{root}(z) u(z)^2 \quad (1)$$

where F_{veg} is the spatially-averaged vegetation drag (m s^{-2}), z is the height from bed (m), F_{stem} and F_{root} are the contributions by stems and roots to F_{veg}, respectively, C_D is the drag coefficient, n_{tree} is the tree density (m^{-2}), $D_{stem,ave}$ is the mean stem diameter (m), a_{root} is the spatially-averaged projected area density of roots (m^{-1}), and u is the flow velocity (m s^{-1}). We represented stems as cylindrical shapes with vertically uniform diameter (Maza et al., 2017) and then calculated the F_{stem} using the cylinder drag model–the same equations introduced by Beudin et al. (2017) (Text S1 and Table 1). Here, we assumed the vertically constant and uniform drag coefficient (C_D) for stems and roots.

2.1.2 Turbulence

In ROMS, the generic length scale (GLS) model is implemented as the turbulence closure, where the equations can represent several two-equation closure models such as k–ε and k–ω models by adjusting the model parameters (Umlauf and Burchard, 2003; Warner et al., 2005). In this manuscript, we present equations in the form of the k–ε model for reference purposes as this is the most studied two-equation closure model for flows in vegetated areas (López and García, 2001; Katul et al., 2004; Defina and Bixio, 2005; King et al., 2012). Beudin et al. (2017) have included an additional term for wake production due to vegetation (P_w) in the equation for turbulence kinetic energy (TKE) as

$$\frac{\partial k}{\partial t} + u\frac{\partial k}{\partial x} = \frac{\partial}{\partial z}\left(\frac{\nu_t}{\sigma_k}\frac{\partial k}{\partial z}\right) + P_s + B + P_w - \varepsilon \quad (2)$$

where k is TKE (m^2 s^{-2}), ν_t is the eddy viscosity (m^2 s^{-1}), σ_k is the turbulent Schmidt number for k (1.0), P_s, B, and P_w represent the production of k by shear, buoyancy, and wakes generated by vegetation (m^2 s^{-3}), respectively, and ε is the turbulent dissipation (m^2 s^{-3}). Similarly, they included an additional term (D_w) in the equation for ε as

$$\frac{\partial \varepsilon}{\partial t} + u\frac{\partial \varepsilon}{\partial x} = \frac{\partial}{\partial z}\left(\frac{\nu_t}{\sigma_\varepsilon}\frac{\partial k}{\partial z}\right) + \frac{\varepsilon}{k}(c_1 P_s + c_3 B - c_2 \varepsilon) + D_w \quad (3)$$

where σ_ε is the turbulent Schmidt number for ε (1.3), c_1 (1.44), c_2 (1.92), and c_3 are the model constants, where the value of c_3 varies depending on the stratification state (Warner et al., 2005), and D_w is the dissipation rate of wakes (m^2 s^{-4}). The wake production rate (P_w) is typically considered equal to the rate of work done by the flow against vegetation drag, i.e., $P_w = F_{veg}u$ (Nepf, 2012). In contrast, the turbulence dissipation rate largely depends on the turbulence length scale in addition to the TKE, which requires a prior knowledge of the turbulence length scale of wakes for correctly predicting the D_w (King et al., 2012; Liu et al., 2017; Li and Busari, 2019).

Previous flume studies for flow through vegetated areas have shown that the stem diameter (or leaf width) is the plausible turbulence length scale of wakes (Tanino and Nepf, 2008; King et al., 2012). In the case of flow in *Rhizophora* mangrove forests, however, there are two potential length scale: stem diameter and root diameter–that could significantly differ from each other (Maza et al., 2017). This variation makes it challenging to parameterize them into one representative length scale of wakes (L in Eq. S6 in Text S2). To resolve this, we partitioned the P_w and D_w into the terms for wakes generated by stems and roots, respectively, as

$$P_w = P_{w,stem} + P_{w,root} = F_{stem}u + F_{root}u \quad (4)$$

$$D_w = D_{w,stem} + D_{w,root} = c_2 \frac{P_{w,stem}}{\tau_{stem}} + c_2 \frac{P_{w,root}}{\tau_{root}} \quad (5)$$

where $P_{w,stem}$ and $P_{w,root}$ ($m^2\ s^{-3}$) are the production of k by stem- and root-generated wakes, $D_{w,stem}$ and $D_{w,root}$ ($m^2\ s^{-4}$) are the dissipation rate of stem- and root-generated wakes, and τ_{stem} and τ_{root} (s) are the time-scale of stem- and root-generated wakes, respectively; these are given by

$$\tau_{stem} = \left(\frac{{L_{stem}}^2}{{c_w}^2 P_{w,stem}}\right)^{1/3} \quad (6a)$$

$$\tau_{root} = \left(\frac{{L_{root}}^2}{{c_w}^2 P_{w,root}}\right)^{1/3} \quad (6b)$$

where L_{stem} and L_{root} (m) are the length scale of stem- and root-generated wakes, respectively, and c_w is the model constant. Here, we set mean stem diameter ($D_{stem,ave}$) and root diameter ($D_{root,ave}$) as L_{stem} and L_{root}, respectively.

We considered c_w in Eq. (6) as a calibration parameter whereas Beudin et al. (2017) gave a value of 0.09. Tanino and Nepf (2008) predicted the TKE for a flow through an array of emergent cylinders with cylinder projected area density, a, and cylinder diameter, d, using $k = \gamma\left(\frac{1}{2}C_D a d\right)^{2/3} u^2$, where γ is the scale coefficient that needs to be empirically determined. We can relate c_w with γ as $c_w = \gamma^{-3/2}$ by applying the k–ε model to a limiting case of a steady, uniform, and neutrally-stratified flow through homogeneous emergent vegetation such that all the terms in Eqs. (2–3) except for k, ε, P_w, and D_w can be neglected (King et al., 2012; Liu et al., 2017). We adjusted the value of c_w so that the corresponding γ value falls within a reported range (0.8–1.6; King et al., 2012; Xu and Nepf, 2020).

2.1.3 Root projected area density

We used the empirical *Rhizophora* root model (*Rh*-root model) developed by Yoshikai et al. (2021) as a predictor of the root projected area density (a_{root}) in Eq. (1). Based on allometric relationships characterized by some site- and species-specific root scaling parameters (α_S, β_S, α_{HR}, β_{HR} in Eq. S7 in Text S3), the *Rh*-root model predicts the vertical profile of root projected area per vertical interval (dz; 0.05 m in this study) for a tree "i" ($A_{root,i}(z)$ (m^2)) from the stem diameter of the tree ($D_{stem,i}$), where the subscript "i" represents the tree index. In short, $A_{root,i}(z)$ is expressed as $A_{root,i}(z) = f(D_{stem,i})$, where f represents a function of the *Rh*-root model (see Text S3 for the details).

The vertical profile of spatially-averaged projected area density of roots in each grid can be calculated as $a_{root}(z) = n_{tree}\sum_{i=1}^{N_{tree}} f\left(D_{stem,i}\right)/(N_{tree}dz)$, where n_{tree} is the tree density (m^{-2}) and N_{tree} is the number of trees in each grid. While some variations in tree sizes (i.e., $D_{stem,i}$), and thereby, $f(D_{stem,i})$ within a grid are expected, it would be convenient if the subgrid-scale variations can be parameterized using a grid-scale parameter for modeling purposes. In this study, we propose that the

mean stem diameter ($D_{stem,ave}$) can be used for the parameterization as $\sum_{i=1}^{N_{tree}} f(D_{stem,i})/N_{tree} \approx f(D_{stem,ave})$, so that $a_{root} \approx n_{tree} f(D_{stem,ave})/dz$.

We investigated the above assumption using tree census data collected from three sites (Bak1, Bak2, and Fuk; see Fig. S1 and Text S4 in the Supporting Information for the map and description of the sites). Using the *Rh*-root model, we computed the vertical distribution of the mean projected area of individuals in the tree census plots, $\sum_{i=1}^{N_{tree}} f(D_{stem,i})/N_{tree}$, and its representation using the mean stem diameter, $f(D_{stem,ave})$, and compared them (Fig. 2). The results demonstrate that the use of $D_{stem,ave}$ can well represent the mean projected area density of individuals for all the three sites regardless of the differences in the forest structures (e.g., stem diameter distribution, tree density) and root scaling parameters (Table S1).

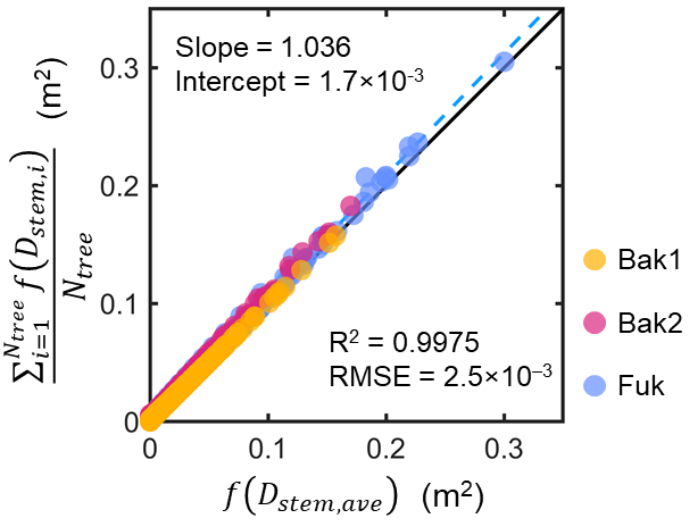

Figure 2. Comparison of the vertical profiles of mean projected area per vertical height interval (*dz*; 0.05 m) of individuals in tree census plots from three sites (Bak1, Bak2, and Fuk), $\sum_{i=1}^{N_{tree}} f(D_{stem,i})/N_{tree}$, and its representation using the mean stem diameter, $f(D_{stem,ave})$, where N_{tree} is the number of *Rhizophora* trees in a plot, $D_{stem,ave}$ is the mean stem diameter of *Rhizophora* trees in the plot, the subscript "*i*" represents the tree index, and *f* represents the function of the *Rhizophora* root model that gives the vertical profile of the root projected area of individuals. The black line indicates the 1:1 line and the blue dashed line indicates the best-fitting line.

2.2 Model testing

We tested the new model implemented in the COAWST against the measurements of flow in a laboratory model of the *Rhizophora* mangrove forest by Maza et al. (2017) and in a planted *Rhizophora* mangrove forest in the field by Yoshikai et al. (2022a). Text S5 provides some descriptions of the implementation of the new model to the COAWST. Both studies have

provided detailed information on vegetation and hydrodynamic parameters that allow us to evaluate the model's performance. Specifically, the mangrove forests in both studies have spatially uniform vegetation distribution due to the uniformly sized and evenly distributed trees (approximately, in the case of the real mangrove forest in Yoshikai et al., 2022a). Moreover, both studies have measured flow structures at a location where the flow is well developed, which eliminates the dependence of flow structures on the proximity to the forest leading edge. Given these conditions, we tested the model using a model grid assuming a schematized mangrove forest with uniform bed elevation and vegetation variables described below, and not with a grid representing the actual geometric/topographic conditions of the flume/field. Table S3 summarizes the measured hydrodynamic variables in Maza et al. (2017) and Yoshikai et al. (2022a), the variables controlled in the model, and the target variables to reproduce for each test case.

We created an orthogonal computational grid of 200 m × 200 m area with a 5-m horizontal resolution for the model runs (Fig. S2). We set 15 vertical layers with approximately uniform layer thickness to be applied to the laboratory-based study of Maza et al. (2017). For the field-based study (Yoshikai et al., 2022a), the number of vertical layers was reduced to 5 because of the shallow water depths. To create a unidirectional flow in the model, we set the eastern and western boundaries of the model domain closed (no water fluxes) and the northern and southern boundaries open (Fig. S2). Then we imposed water level differences between the northern and southern boundaries to drive the flow based on the pressure gradient, where the water fluxes through the boundaries are given to equate the local pressure gradient and the drag force (bed + vegetation). The model was run without wind in the simulation. When the steady state of flow was attained in the simulation, we compared the flow condition at the center of the model domain with the measured values (Fig. S2). This means that the actual time-series of the flow during the tidal cycle was not reproduced when the model was applied to the field mangrove forest; rather, steady states of flow were created for each flow measurement. Table 1 summarizes the key vegetation and hydrodynamic parameters for each test case.

We set different objectives for the applications of the model to laboratory- and field-based studies. The main objective of applying the model to a laboratory-based study is to examine the effectiveness of the formulations for the drag and turbulence terms (Eq. (1)–(6)), which were newly implemented in the COAWST to predict the flow structures in the *Rhizophora* mangrove forest, compared to the ones predicted by the cylinder drag model. Here, we consider the vegetation frontal area density (a) as a known parameter. In contrast, the parameter a is usually unknown and needs to be predicted in the case of mangrove forests in the field. Hence, the main objective of the application to the field-based study is to examine the effectiveness of the proposed framework (Fig. 1) that includes the *Rh*-root model – the predictor of a – in the COAWST, compared to the drag parameterizations proposed in previous studies. Table 2 summarizes the different model configurations tested to represent the impact of *Rhizophora* mangroves for applications to the laboratory- and field-based studies. Below we describe an overview of the measurements by Maza et al. (2017) and Yoshikai et al. (2022a) and the model settings.

Table 1. Vegetation and hydrodynamic parameter settings for model testing against flume experiments (Exp 1 and 2) in Maza et al. (2017) and field measurement in Yoshikai et al. (2022a). Figure S3 shows the location where the values of vegetation and hydrodynamic variables in the table were derived in Yoshikai et al. (2022a). Note that the values of vegetation and hydrodynamic variables in the flume in Maza et al. (2017) were converted to the real scale. The row for γ shows the values that best fit the measurements within the range of 0.8–1.6.

Parameter	Exp 1	Exp 2	Field
Stem diameter (D_{stem}, m)	0.2	0.2	0.066 [a]
Root diameter (D_{root}, m)	0.038	0.038	0.030 [a]
Maximum root height (HR_{max}, m)	2.01	2.01	1.10 [a]
Tree density (n_{tree}, m^{-2})	0.072	0.072	0.36
Drag coefficient (C_D)	0.8	0.8	1.0
Water depth (h, m)	3.0	1.79	0.14–0.53 [b]
Cross-sectional mean velocity (U, m s^{-1})	0.31	0.58	[c]
Scale coefficient (γ)	1.5	0.9	0.8

[a] Mean value at the measurement site.
[b] Water depth varies depending on the tidal phase (see Fig. 6a, e).
[c] One of the target parameters for model prediction.

Table 2. Tested model configurations to represent the impact of *Rhizophora* mangroves against flume experiments (Exp1 and 2) in Maza et al. (2017) and field measurement in Yoshikai et al. (2022a). n_{tree}: tree density; n_v: cylinder density; $D_{stem,ave}$: mean stem diameter; b_v: cylinder density; a_{root}: root projected area density; $D_{root,ave}$: mean root diameter; z_0: bed roughness length; N_{layer}: number of vertical layers of model grid.

Test case	Model configuration	Parameter settings					
		n_{tree} or n_v (m^{-2})	$D_{stem,ave}$ or b_v (m)	a_{root} (m^{-1})	$D_{root,ave}$ (m)	z_0 (m)	N_{layer}

Flume experiment	*Rh* model	0.072 (n_{tree})	0.2 ($D_{stem,ave}$)	Measured value [a]	0.038	0.5×10^{-3} [e]	15
	Cylinder model for Exp1	1.22 (n_v)	0.038 (b_v)	-	-	0.5×10^{-3} [e]	15
	Cylinder model for Exp2	1.76 (n_v)	0.038 (b_v)	-	-	0.5×10^{-3} [e]	15
Field measurement	*Rh* model with actual a_{root}	0.36 (n_{tree})	0.066 ($D_{stem,ave}$)	Measured value [b]	0.030	0.5×10^{-3}	5
	Rh model with modeled a_{root}	0.36 (n_{tree})	0.066 ($D_{stem,ave}$)	Modeled value [c]	0.030	0.5×10^{-3}	5
	Cylinder model (sparse)	13.5 (n_v)	0.030 (b_v)	-	-	0.5×10^{-3}	5
	Cylinder model (dense)	32.3 (n_v)	0.030 (b_v)	-	-	0.5×10^{-3}	5
	Generic root model	0.36 (n_{tree})	0.066 ($D_{stem,ave}$)	Eq. (S11) [d]	0.010	0.5×10^{-3}	5
	Increased z_0	-	-	-	-	0.02	3
	No vegetation	-	-	-	-	0.5×10^{-3}	5

[a] Corresponds to the value of black markers minus $n_{tree}D_{stem,ave}$ in Fig. 3a.
[b] Corresponds to the value of black markers minus $n_{tree}D_{stem,ave}$ in Fig. 3b.
[c] Corresponds to the value of blue markers minus $n_{tree}D_{stem,ave}$ in Fig. 3b.
[d] Corresponds to the value of light green markers minus $n_{tree}D_{stem,ave}$ in Fig. 3b.
[e] Assumed value.

2.2.1 Application to a laboratory-based study

The model *Rhizophora* mangrove forest created in the flume by Maza et al. (2017) was 1/12th, while we ran our model in a real scale, i.e., we converted the velocities in the flume to the real scale by keeping the Froude number (Table 1). The real-scale vertical profile of vegetation projected area density (a) is shown in Fig. 3a. Maza et al. (2017) fabricated the root systems based on the data in Ohira et al. (2013) and distributed the model trees in-line in the flume. Maza et al. (2017) created two flow conditions by varying the water depth (h) and cross-sectional mean velocity (U) (Exp 1 and 2; Table 1) and measured the vertical profiles of velocities and TKE at five lateral positions in the model forest, at which flows were fully developed (Table S3). We averaged the data taken at the five positions to estimate the spatial average of the velocity and TKE to be compared with the model output.

We imposed the real-scale vertical profile of a examined in Maza et al. (2017) (black markers in Fig. 3a) over the model domain. This means that the *Rh*-root module that predicts a_{root} was not applied for the simulations performed here. We

optimized the water levels at the boundaries to create the same flow conditions (h and U) at the center of the model domain as the ones in Exp 1 and 2, respectively.

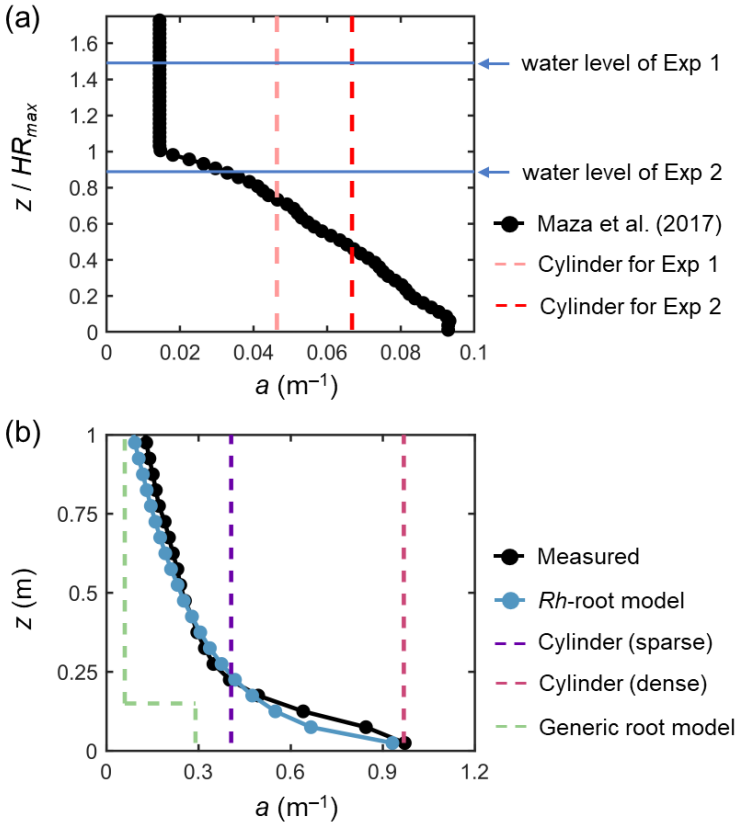

Figure 3. Vertical profiles of vegetation projected area density, a, in (a) a model *Rhizophora* mangrove forest examined by Maza et al. (2017) and (b) a real *Rhizophora* mangrove forest examined by Yoshikai et al. (2022a), where the values were calculated with dz = 0.05 m vertical interval (markers). HR_{max} is the maximum root height (2.01 m in Maza et al. (2017); Table 1). The modeled a using the *Rh*-root model in panel "b" is given by the *Rhizophora* root module using the parameters shown in Tables 1 and S1 (for Bak2). The projected area density of cylinder arrays (in panels "a" and "b") as well as the a predicted using the generic mangrove root model (in panel "b"), which were used for comparison with the new model to represent the impacts of *Rhizophora* mangroves, is also shown (dashed lines).

We used a value of 0.8 for the drag coefficient (C_D) in the model (Table 1), the value of which was derived in fully developed flows with high Reynolds numbers (> 230) by Maza et al. (2017). The value of the bottom roughness (z_0) in the flume is unknown; hence we gave 0.5 mm to z_0, which is the value derived in the field-based study (see Section 2.2.2). Due to the uncertainty of the bottom roughness, we did not include the modeled near-bed velocity and TKE for comparison with the

measurements, above which the velocity and TKE were insensitive to the bottom roughness. Another unknown parameter is the scale coefficient in the turbulence closure, γ (= $c_w^{2/3}$; see Section 2.1.2). We run the model by varying γ in a reported range (0.8–1.6) with an interval of 0.1 to seek a value that produced the best fit with the measurement, mostly for the TKE profile. Figure S4 provides the model sensitivity to the varying γ for the prediction of TKE profiles.

In addition to the simulation using the actual *a* (black markers in Fig. 3a), referred to as the "*Rh* model", we tested the use of the cylinder drag model, referred to as the "cylinder model" (Table 2). We defined the cylinder array for Exp 1 and 2, respectively, where the cylinder projected area density was set equal to the depth-average of the actual *a* for each case (dashed lines in Fig. 3a); we set the cylinder diameter equal to the root diameter of the model *Rhizophora* trees (0.038 m; Table 1). Cylinder height was set well higher than the water level to create the condition that cylinders span the entire water column – this also applies to the cylinder drag model examined in the next section.

2.2.2 Application to a field-based study

Yoshikai et al. (2022a) measured vegetation and hydrodynamic parameters at 17-year-old planted stands of *Rhizophora apiculata* in a mangrove forest locally known as Bakhwan Ecopark in Aklan, Philippines (Fig. S3). The site corresponds to Bak2 in Fig. 2. Like in the flume condition of Maza et al. (2017), approximately uniformly sized trees are evenly distributed. The measured spatially averaged vegetation projected area density (*a*) at the site is shown in Fig. 3b. Due to the higher complexity of the root systems and higher tree density (Table 1), the *a* near the bed showed almost 10 times higher value than the one in Maza et al. (2017) (Fig. 3). Yoshikai et al. (2022a) conducted hydrodynamic measurements during ebb tides on September 10 and 11, 2018 that corresponded to spring tide conditions. The measured parameters were water depth, spatially averaged velocity profile (based on measurements at four locations), water surface slope along a major flow direction, and bed shear stress (Table S3). The flow at the site is considered fully developed.

We imposed the measured water surface slope at the boundaries to drive the flow, where the water depths at the boundaries were adjusted to realize the same water depth at the center of the model domain as the measurement. We used a value of 1.0 for the drag coefficient (C_D) and 0.5 mm for the bottom roughness (z_0) based on the results in Yoshikai et al. (2022a) (Table 1). As in the previous section, we changed the value of γ in a reported range (0.8–1.6) with an interval of 0.1 to seek a value that produced the best fit with the measured velocity profile. Note that the TKE profile has not been measured in the field, thus it could not be validated.

We tested seven different model configurations (Table 2): *Rh* model using the measured values for a_{root} (actual *a*; black markers in Fig. 3b), *Rh* model using the modeled a_{root} (blue markers in Fig. 3b), cylinder model using two different cylinder densities (sparse and dense; purple and red dashed lines in Fig. 3b), use of the other predictive model for *Rhizophora* root structures used in Xie et al. (2020) as the predictor of a_{root} in Eq. (1) (termed as generic root model; green dashed line in Fig. 3b), increased bed roughness (z_0), and a case without imposing the vegetation drag (no vegetation). Among these, the proposed framework (Fig. 1) was used for the case *Rh* model using the modeled a_{root} (the *Rhizophora* root module provided the a_{root} in

the simulation) with input parameters of measured mean stem diameter ($D_{stem,ave}$) and tree density (n_{tree}). We set the sparse cylinder case based on Horstman et al. (2013) who suggested the use of vegetation geometry measured at a height of around 0.25 m for cylinder array approximation. We set the dense cylinder array to produce an equivalent resistance to Manning's coefficient of 0.14 at a water depth of 0.5 m, a value often used to represent the drag by mangroves (e.g., Zhang et al., 2012; Menéndez et al., 2020). The generic root model used in Xie et al. (2020) predicts the mangrove root structure (a_{root}) as an array of vertical cylinders with a fixed diameter (D_{root}) and height (H_{root}) from a given stem diameter and tree density (see Text S6 for the model details). We use the term "generic" because Xie et al. (2020) used this model to represent root structures of several different mangrove genera including *Rhizophora*. Here, we used the same parameter values for D_{root} and H_{root} as the ones used in Xie et al. (2020) for *Rhizophora* root structures: D_{root} = 0.01 m and H_{root} = 0.15 m. The vegetation frontal area (stem + root) predicted by the generic root model using measured mean stem diameter ($D_{stem,ave}$ = 0.066 m) and tree density (n_{tree} = 0.36 m^{-2}) is shown in Fig. 3b. Here, the predicted a_{root} is used for calculating the drag by roots in Eq. (1). In addition, $D_{stem,ave}$ = 0.066 m and D_{root} = 0.01 m were applied for L_{stem} and L_{root} in the turbulence dissipation term of Eq. (6) (Table 2). For the case of increased z_0, we reduced the number of vertical layers from 5 to 3 and set z_0 = 0.02 m (Table 2; see Text S7 for the details of bed shear stress calculation and the choice of the value). We note that the z_0 value equivalent to Manning's coefficient of 0.14 at 0.5 m water depth is z_0 = 0.22 m, but we were able to increase the value up to 0.02 m due to the numerical limitation of the logarithmic velocity profile assumption implemented in the COAWST (Eq. (S13)). For the case without vegetation, z_0 is kept as 0.5×10^{-3} m, the same as the other vegetated cases. In the increased z_0 and the no vegetation cases, the bed shear stress is the main force to equate with the imposed pressure gradient.

3 Results

3.1 Comparison with a laboratory-based study

Figure 4 shows a comparison of the modeled and measured vertical profiles of velocity (u) and TKE (k) normalized by cross-sectional mean velocity (U) for Exp 1 and 2, the conditions examined by Maza et al. (2017). The profile of normalized velocity was reasonably predicted by the *Rh* model (Fig. 4a, c), especially at the lower part of the root system (i.e., $z/HR_{max} <$ 0.6) in Exp 1 where the velocity was greatly attenuated compared to the upper part or above the root system (Fig. 4a). The higher values of the γ lead to more homogeneous velocity profiles because of the enhanced vertical momentum exchange by the elevated TKE, while the sensitivity to the varying γ was not significant. The *Rh* model also predicted well the overall trend of the normalized TKE profile measured by Maza et al. (2017) for both Exp 1 and 2 by adjusting the value of γ (Fig. 4b, d). Notably, the *Rh* model captured well the distinct vertical variations in TKE observed in Exp 1 when γ = 1.5 (Fig. 4b), while for Exp 2, the best fit was obtained when γ = 0.9 (Fig. 4d). Overall, γ = 1.2 produced the smallest total error of Exp 1 and 2 between the model and measured values (Fig. S4). It under- and overestimated the TKE averaged over the measurement section by about 20 and 40 % for Exp 1 and 2, respectively (Fig. 4b and d), which is generally a fairly good agreement for predicting TKE.

In contrast to the *Rh* model, the cylinder model predicted the nearly uniform vertical profile of velocity except for the region close to the bed both for Exp 1 and 2 and largely deviated from the measurements (Fig. 4a and c). The TKE predicted by the cylinder model also showed a nearly uniform vertical profile (Fig. 4b and d). While the cylinder model showed comparable TKE with the *Rh* model at the lower part of the root system (i.e., $z/HR_{max} < 0.4$) for both cases, it showed a significantly smaller TKE at the upper region from the *Rh* model and the measurement.

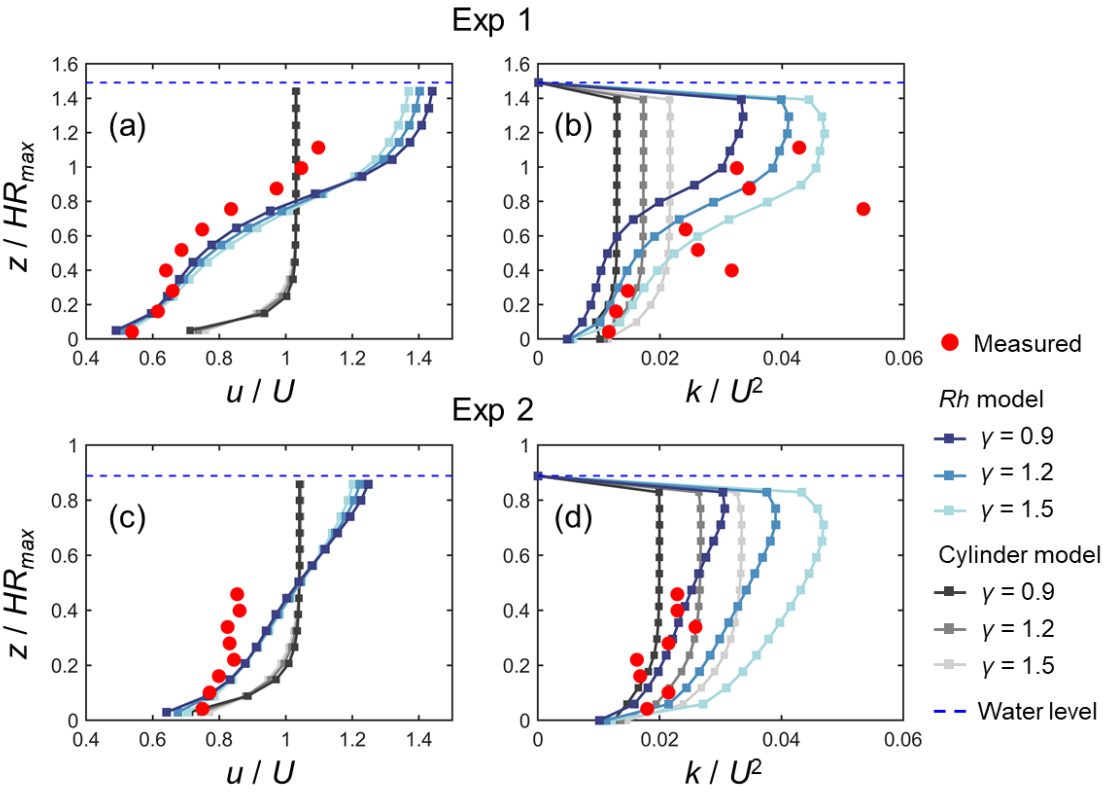

Figure 4. Comparison of the vertical profiles of (temporally and spatially averaged) velocity (u) and turbulent kinetic energy (k) normalized by the cross-sectional mean velocity (U) predicted by the COAWST with different model configurations (*Rh* model and cylinder model) and with different γ values, and measurement by Maza et al. (2017) for (a, b) Exp 1 and (c, d) Exp 2. HR_{max} is the maximum root height. Data on the measured values are provided in Table S4.

3.2 Comparison with a field-based study

Figure 5 shows the comparison of modeled velocity profiles with measurements by Yoshikai et al. (2022a) for some selected tidal phases in a *Rhizophora* mangrove forest (Bakhawan Ecopark). The *Rh* model using the measured profile of root projected area density (actual a_{root}) predicted well the overall trend of measured velocity profiles in various tidal phases (Fig.

5a). However, the model seemed to have underestimated the velocity attenuation from the surface to the bottom, which resulted in slightly higher near-bottom velocity and/or lower near-surface velocity compared to the measurement. Here, the value of γ was chosen as 0.8 from the range 0.8–1.6 (Table 2), which produced the best fit with the measured velocity profile. The *Rh* model using the modeled a_{root} provided by the *Rhizophora* root module showed comparable performance with the use of actual a_{root} in predicting the velocity profile (Fig. 5a). However, although not significant, the use of modeled a_{root} tended to further underestimate the velocity attenuation from the surface to the bottom due to the underestimation of a_{root} near the bed by the *Rh*-root model (Fig. 3b).

The cylinder model with sparse arrays showed comparable velocities with measurements near the water surface, but significantly overestimated the velocities near the bed (Fig. 5b). Alternatively, the dense arrays showed comparable velocities near the bed, but significantly underestimated the velocities near the water surface (Fig. 5c). The use of generic root model as a predictor of a_{root} in Eq. (1) led to significant overestimation of velocities over the depths (Fig. 5d) due to the significantly underestimated vegetation projected area density (Fig. 3b). The approximation of mangrove drag in the z_0 (increased bed roughness case) predicted the significant attenuation of flow velocity from the surface to the bottom due to the large bottom friction, which did not well represent the actual conditions of velocity profile in the *Rhizophora* mangrove forest (Fig. 5e). The condition without imposing vegetation drag effects led to a large overestimation of the velocities, approximately 3–4 times larger than the measurements (Fig. 5f).

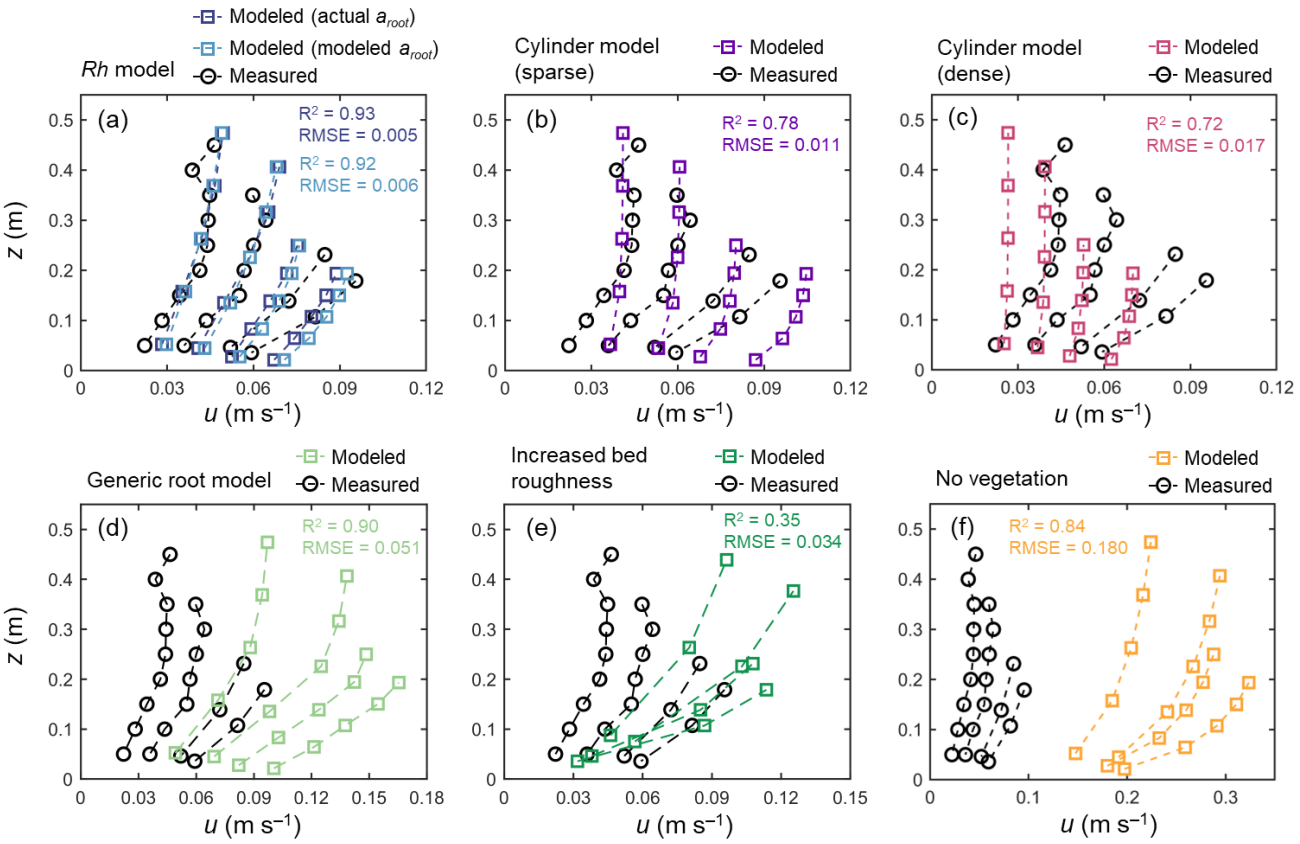

Figure 5. Comparison of the vertical profiles of velocity (u) predicted by the COAWST employing (a) *Rh* model using actual and modeled root projected area density profile (a_{root}), (b) cylinder model with sparse and (c) dense array, (d) generic root model, (e) increased bed roughness as an approximation of vegetation drag, and (f) without imposing vegetation drag (no vegetation), and measurement by Yoshikai et al. (2022a) for some selected tidal phases during the measurement period. The root mean square error (RMSE) and R^2 values of the modeled u against the measured data are also shown, for which computation of the predicted value at the height of the measurement point was obtained by the interpolation of u computed at adjacent vertical layers. Data on the measured values are provided in Table S5.

A fairly good reproduction of tidal flows by the *Rh* model can also be seen in agreement with the measurement for the time-series of channel-mean velocity (U), (spatially averaged) velocity at z = 0.05 m (u_{bottom}), and bed shear stress (τ_{bed}) during the 2-days measurement period (Fig. 6). Note that we estimated the model prediction of velocity at z = 0.05 m from linear interpolation of velocities computed at adjacent vertical layers. The u_{bottom} was generally overestimated by about 15 % (Fig. 6c, g), as also seen in Fig. 5a. As a result, the τ_{bed} was overestimated by about 30 % by the model, which is still a reasonable

agreement (Fig. 6d, h). As demonstrated in Fig. 5a, the *Rh* model employing the modeled a_{root} also showed a comparable performance for the time-series data (Fig. 6).

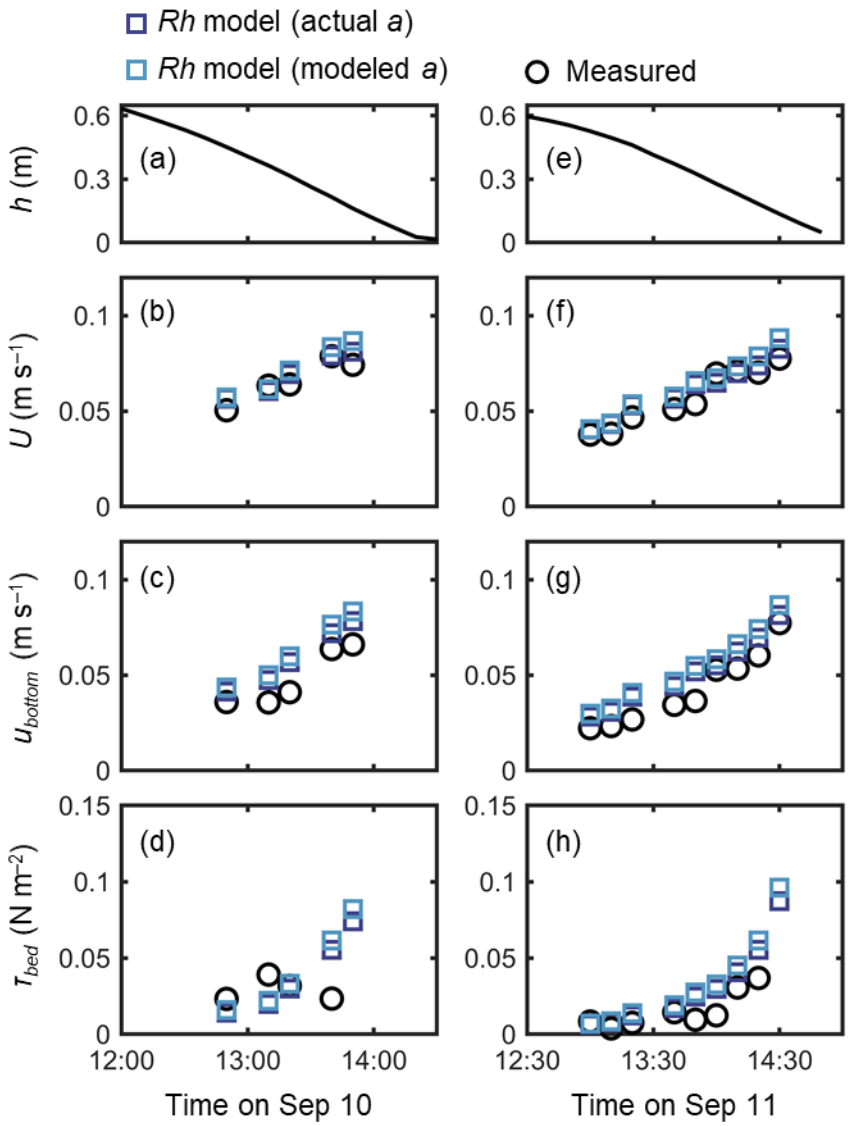

Figure 6. Time-series of (a, e) measured water depth (h), measured and predicted (b, f) cross-sectional mean velocity (U), (c, g) (spatially averaged) velocity at z = 0.05 m, and (d, h) bed shear stress (τ_{bed}) during the two-days measurement in Bakhawan Ecopark. The measured values are from Yoshikai et al. (2022a) and the predicted values are obtained through the COAWST employing the *Rh* model using actual and modeled root projected area density profile (a_{root}). Data on the measured values are provided in Table S6.

The cylinder model with a sparse array led to a significant overestimation trend of the U, u_{bottom}, and τ_{bed} over the tidal phases especially when the water depth decreased (Fig. 7). The cylinder model with a dense array led to the underestimation of U in most of the tidal phases but showed an agreement with the measurement for u_{bottom} and τ_{bed} (Fig. 7). The use of generic root model resulted in consistently higher U, u_{bottom}, and τ_{bed} compared to the measured values (Fig. 8), similar to the trend seen in Fig. 5d. Although the case using the increased z_0 showed a large overestimation of flow velocities as much as the case using the generic root model when the water depth is relatively high (e.g., h > 0.3 m), it approached the measured values with decreasing water depth (Fig. 8); we will discuss these contrasting results in the following section. Because the bed drag is the main force to counteract the imposed pressure gradient in the increased z_0 case, the τ_{bed} showed a large overestimation over the tidal phases as expected (Fig. 8c, f). The model without imposing vegetation drag led to a large overestimation of these parameters over the tidal phases (Fig. S5), similar to the result shown in Fig. 5f.

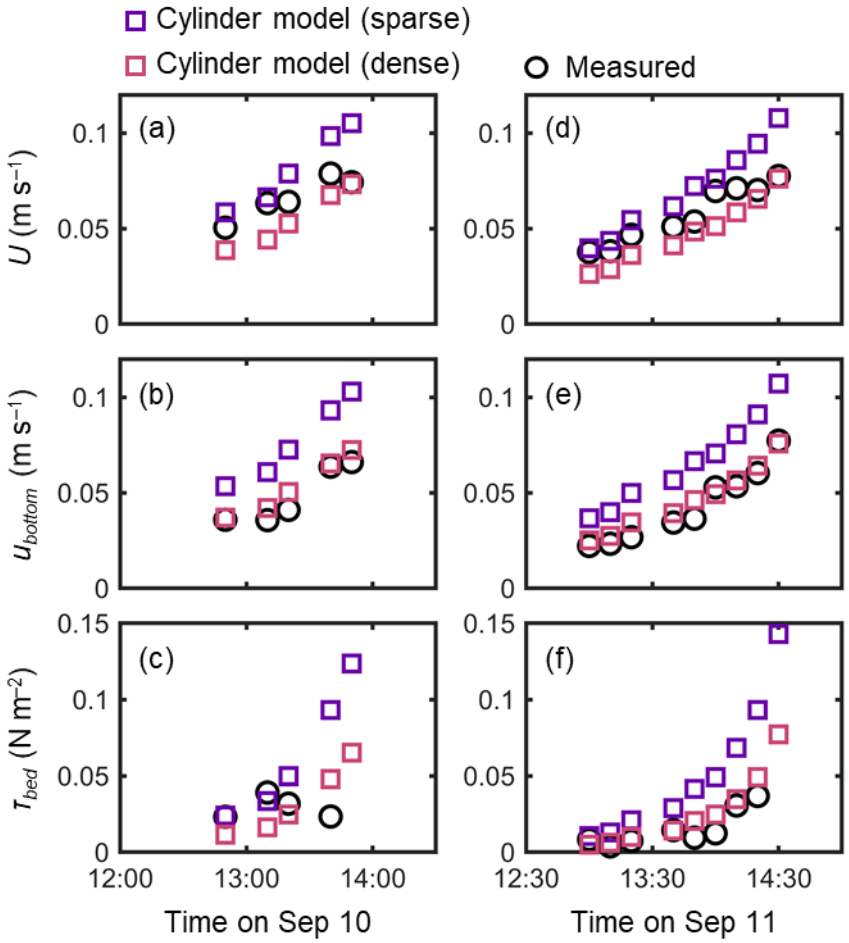

Figure 7. Time-series of measured and predicted (a, d) cross-sectional mean velocity (U), (b, e) (spatially averaged) velocity at z = 0.05 m, and (c, f) bed shear stress (τ_{bed}) during the two-days measurement in Bakhawan Ecopark. The measured values are from Yoshikai et al. (2022a) and the predicted values are obtained through the COAWST employing the cylinder model with sparse and dense arrays.

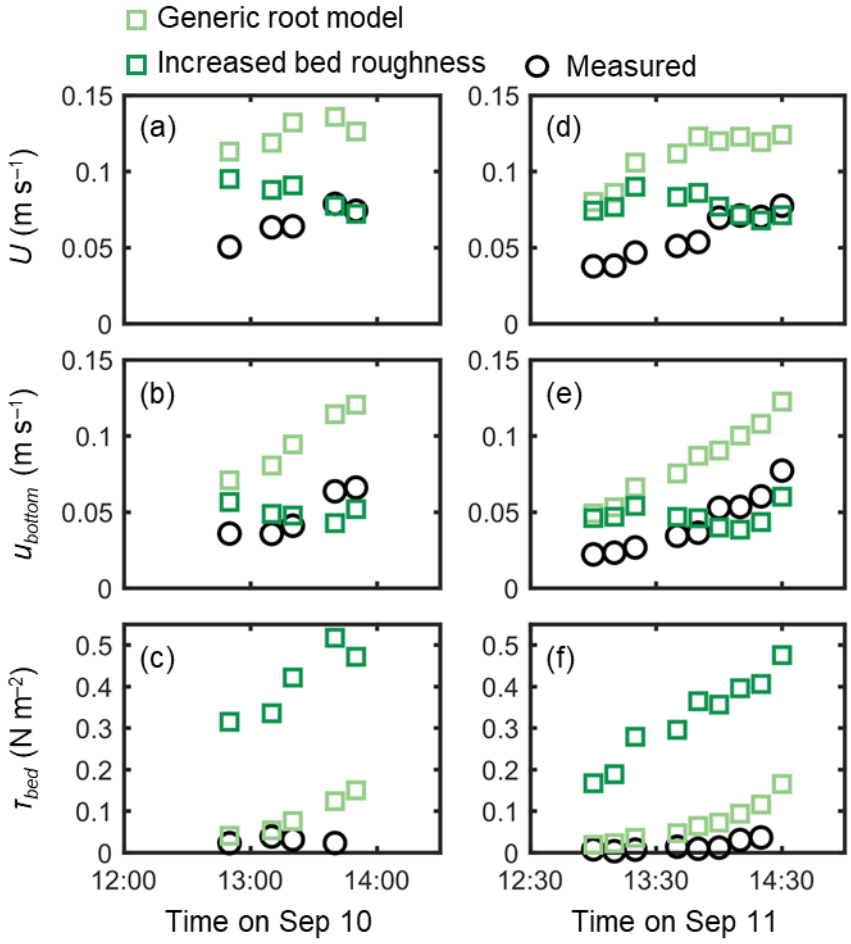

Figure 8. Time-series of measured and predicted (a, d) cross-sectional mean velocity (U), (b, e) (spatially averaged) velocity at z = 0.05 m, and (c, f) bed shear stress (τ_{bed}) during the two-days measurement in Bakhawan Ecopark. The measured values are from Yoshikai et al. (2022a) and the predicted values are obtained through the COAWST employing the generic root model and the increased bed roughness as an approximation of drag by mangroves, respectively.

4 Discussion

4.1 Performance of the previously proposed drag parameterization

Due to the general lack of information on the vertically varying projected area of the complicated root systems, the drag by *Rhizophora* mangroves has been represented by the increased Manning's roughness coefficient values (e.g., Zhang et al., 2012) or an array of cylinders with arbitrary cylinder density (Horstman et al., 2013; Xie et al., 2020) in hydrodynamic models with 2D configuration. We evaluated these drag parameterizations using the cylinder array or increased bed roughness approximation in 3D configuration (dashed lines in Fig. 3 for the cylinder arrays). Consistent with previous studies (Liu et al., 2008; King et al., 2012), the cylinder array approximations showed the vertically uniform velocity and TKE profile except near the bed, which largely deviated from the measurements (Figs. 4 and 5). Moreover, for the tidal flows with changing water depth, the two different cylinder array configurations (sparse and dense) failed to capture the velocity changes over the tidal phases (Fig. 7) due to the inability to capture the changes in submerged vegetation projected area of *Rhizophora* mangroves.

The generic mangrove root model used in Xie et al. (2020) predicts the *Rhizophora* root system as an array of vertical cylinders having a fixed height and diameter. However, the root system structures of *Rhizophora* mangroves cannot be simply approximated as the array of vertical cylinders as shown in Fig. 3b. Although the shape of the velocity vertical profiles predicted using the generic root model resembles that of observed profiles as indicated by the high R^2 value in Fig. 5d, the model failed to predict the absolute values as indicated by the high RMSE due to the significant underestimation of the a (Fig. 3b). Because the shape of a predicted by the generic root model is similar to those of submerged vegetations, it is expected that the velocity inflection at the top of the root zone ($z = H_{root}$) will form as the projected area density of roots (a_{root}) further increases (e.g., King et al., 2012; Nepf 2012), which would further deviate the results from the actual velocity profiles.

Unlike the cylinder array approximations including the generic root model where the total projected area of submerged cylinders changes with the water depth, the approximation with increased bed roughness inherently assumes the invariant area of obstructions to flows. This means that the impact of bed roughness on flow velocity becomes more significant as the water depth decreases. This effect can be seen in the prediction of cross-mean flow velocity (U) at different tidal phases where the predicted U, which was largely overestimated under the relatively high water depth (h > 0.3 m), approached the measured values as the water depth decreases, unlike the case using the generic root model (Fig. 8b, e). The approximation with increased bed roughness leads to the large overestimation of τ_{bed} (Fig. 8c, f), hence making it not suitable for applications to sediment transport modeling in mangrove forests. Overall, none of the previously proposed drag parameterization captured well the flow structures in the *Rhizophora* mangrove forests examined in this study.

4.2 Performance of the new model

We proposed a new drag and turbulence model for flows in *Rhizophora* mangrove forests that works on the 3D hydrodynamic model, ROMS, and implemented in the COAWST. The model explicitly accounts for the vertically varying

projected area of the root systems for drag force and TKE production in 3D configuration. In addition, the model accounts for the two different length-scales of wakes (roots- and stem-generated wakes) in the turbulence closure model (k–ε model in this study), an aspect none of the modeling studies has examined yet (e.g., López and García, 2001; King et al., 2012). With the relatively simple modifications made to the equations introduced by Beudin et al. (2017) (Eqs. 1, 4–6), our results showed significantly improved reproducibility of ROMS for the vertical profiles of velocity and TKE, and velocity changes over the tidal phases in *Rhizophora* mangrove forests (Figs. 4, 5, and 6). The new model also reasonably predicted the bed shear stress together with these parameters (Fig. 6d and h). Although some studies have accounted for the vertically varying vegetation projected area in hydrodynamic models for salt marshes (Temmerman et al., 2005) or mangrove forests with *Rhizophora* stands (Horstman et al., 2013, 2015), the efficacy of accounting for the vegetation 3D structures in the model has not been demonstrated. Overall, this is the first modeling study to introduce the realistic representation of the influences of *Rhizophora* mangrove morphological structures on the flow that was validated with existing data. The good performance of the model in both the model- and real-*Rhizophora* mangrove forests suggests the model's applicability to forests having the vegetation density a in the range of 0.09–0.9 m^{-1} near the bed (Fig. 3) and an in-line tree distribution like planted mangrove forests. However, the applicability to forests having $a > 0.9$ m^{-1} and/or heterogeneous tree sizes and distribution, a condition often observed in natural mangrove forests, needs further investigation in future studies.

The laboratory-based study of Maza et al. (2017) provided valuable data for evaluating the new model for TKE in a *Rhizophora* mangrove forest, which is currently unavailable from field-based studies. They observed the elevated TKE at the upper root zone and above the root zone ($z/HR_{max} > 0.5$; Fig. 4b). Maza et al. (2017) discussed the TKE production by shear (P_s in Eq. 2) as one of the main reasons for the elevated TKE. However, we found that the different dominance of the root- and stem-generated wakes over the depth can explain these observations. For instance, the lower root zone that is dominated by root-generated wakes with length-scale set as root diameter (0.038 m; Table 2) resulted in a higher dissipation rate (Eq. 6a), thereby lower TKE (Fig. 4b). On the other hand, the higher root zone dominated by stem-generated wakes with length-scale set as stem diameter (0.2 m; Table 2) resulted in a lower dissipation rate (Eq. 6b), thereby higher TKE (Fig. 4b). This result is similar to the observation by Xu and Nepf (2020) that found vertically varying turbulence integral length-scale in a canopy of a salt marsh plant *Typha*. Without accounting for the two different length scales, the model failed to reproduce the TKE profile while the velocity profile remained similar, suggesting the minor importance of shear production in reproducing the TKE (Fig. S6). The model also predicted the gradually increasing TKE upwards in the lower root zone ($z/HR_{max} < 0.5$), which is consistent with the measurements (Fig. 4b, d). While the model showed good reproducibility of the TKE profile, it should be noted that different γ values produced the best fit with the measurement for Exp1 and Exp2 (Fig. 4b, d). At this moment, the exact explanation for this observation is yet to be determined, whether it can be attributed to measurement uncertainty or processes that were not represented in the model. Further research on the turbulence structures in *Rhizophora* mangrove forests is needed. Unlike the TKE profiles predicted for the model mangrove forest, the TKE predicted for the field mangrove forest (Bakhawan Ecopark) having much higher vegetation complexity (higher a; Fig. 3) showed nearly uniform vertical profiles (Fig. S7); these

results cannot be validated at this moment due to lack of necessary data. Field studies on turbulence structures are likewise needed in this sense.

From the results shown, we highlighted the importance of accounting for the vertically varying projected area of the root systems with 3D configuration for capturing the flow structures (Figs. 4–8). The model predictability is therefore dependent on the root projected area, which is typically unknown and labor-intensive to measure (Yoshikai et al., 2021). For the practical use of the model, we implemented in COAWST an empirical model for the *Rhizophora* root system (*Rh*-root model; Fig. 1) with parameterization of subgrid-scale tree variations (Fig. 2) that enables the model application without rigorous measurements of root structures. The simulation for flows in Bakhawan Ecopark using the modeled a_{root} provided by the *Rhizophora* root module showed almost identical results to the one using the measured a_{root} in the field (Figs. 5 and 6). This indicates the applicability of the model framework for predicting the flows in real *Rhizophora* mangrove forests. The grid-scale parameters required are mean stem diameter ($D_{stem,ave}$) and tree density (n_{tree}), which are basic information collected during tree census surveys (Simard et al., 2019; Suwa et al., 2021). Although the process of collecting these spatial data exceeds the scope of the study, we expect that even remotely sensed data such as airborne LiDAR (Jucker et al., 2017; Dai et al., 2018) or UAV optical imagery (Otero et al., 2018), which can detect basic tree features (e.g., tree height and crown width) that have a strong relationship with stem diameter (Jucker et al., 2017; Azman et al., 2021), can provide such information effectively. Obtaining the root scaling parameters requires field surveys (Fig. 1); however, these parameters can be relatively easily obtained by sampling 10–20 trees at the site (see Yoshikai et al., 2021, 2022a for the procedure). The collection of these data is far less exhaustive than extensively measuring the vertical profile of a_{root} in the area of interest as done by Horstman et al. (2015). Therefore, the model presented in this study may achieve a realistic forest-scale numerical modeling of flows in *Rhizophora* mangrove forests in the field.

4.3 Further model improvement

In order to extend the application of the presented model to sediment transport modeling, an accurate representation of vegetation impacts on both mean flow and turbulence structures that control sediment horizontal flux, retention/erosion, and turbulent mixing, is of primary importance (Nardin and Edmonds, 2014; Xu et al., 2022). Specifically, the greatly reduced near-bed velocity compared to the upper region that may significantly contribute to the sediment retention function of *Rhizophora* mangroves may be a key factor for the sediment transport modeling in this kind of forest, which was captured by the new model only (*Rh*-model in Figs. 4–5). While we expect the improved prediction of the sediment transport process in *Rhizophora* mangrove forests given the improved prediction of overall flow structures using the presented new model, future studies on model application and validation with the field data on sedimentary processes are needed.

Several recent laboratory-based studies have shown that the turbulence generated by vegetation could contribute to sediment erosion, and in that case, TKE may be a better predictor of erosion rate than bed shear stress (Tinoco and Coco, 2016; Yang and Nepf, 2018; Liu et al., 2021). Currently, most numerical models evaluate sediment erosion based on bed shear stress

even for the region with vegetations (e.g., Zhu et al., 2020; Breda et al., 2021; Zhang et al., 2022). Accounting for the impact of vegetation-generated turbulence on the sediment erosion in the model may be the next step to better represent the sediment transport process in *Rhizophora* mangrove forests, where the presented model has the potential to contribute to it. Yet, the insights into the effects of turbulence on sediment erosion in *Rhizophora* mangrove forests are very limited at present, necessitating further laboratory- and field-based studies.

In order to predict the long-term geomorphic evolution of mangrove forests, the interactive feedback of vegetation-flow-sediment needs to be precisely simulated (van Maanen et al., 2015; Rodríguez et al., 2017; Xie et al., 2020). This process involves dynamic vegetation models that can capture long-term changes in root structure complexity in accordance with forest growth/development (e.g., Xie et al., 2020)–a process poorly represented in previous studies in the case of *Rhizophora* mangrove forests. An advantage of the proposed model is that the root structures of *Rhizophora* mangroves are allometrically predicted in the hydrodynamic model from the basic forest structural variables–mean stem diameter and tree density, of which long-term dynamics can now be predicted using dynamic vegetation models for mangroves (e.g., Yoshikai et al., 2022b). The coupling of the hydrodynamic-sediment transport model and the dynamic vegetation model is one of the next challenges that will advance our understanding of the long-term geomorphic evolution in mangrove forests.

5 Concluding remarks

Modeling flow in *Rhizophora* mangroves has been challenging due to their complex root structures. This manuscript presents a new model to represent the impacts of *Rhizophora* mangroves on flow implemented in the COAWST model framework toward a better understanding of hydrodynamics in mangrove forests. The new model explicitly accounts for the effect of the three-dimensional root structures on drag and turbulence as well as the two potential length scales of vegetation-generated turbulence. We showed that the new model significantly improves the prediction of velocity and TKE in *Rhizophora* mangrove forests compared to the conventional approximations of the impact of *Rhizophora* mangroves using cylinder array or increased bed roughness. Specifically, the greatly attenuated near-bed velocity and the consequently lowered bed shear stress due to the high root density at the lower portion of the root systems are captured by the new model only. This has an important implication when expanding the model to simulate sediment transport. Thus, accounting for the realistic morphological structures of *Rhizophora* mangroves in the hydrodynamic model with a three-dimensional configuration is important. While obtaining information on root structures in the field could be challenging, the new model is now feasible in its application due to the incorporation of the empirical model for *Rhizophora* root structures to the COAWST. The model developed here may thus serve as a fundamental tool to advance our understanding of the hydrodynamics and related transport processes in *Rhizophora* mangrove forests with complex root structures.

Code and data availability

The model codes, input data, and run scripts are available at https://zenodo.org/record/7974346 (Yoshikai, 2022).

Author contributions

MY, TN, and KN designed the study and developed the model proposed in the manuscript. MY made the necessary modifications to the model code of the COAWST and performed the analyses. TN and KN contributed to the result interpretation. MY wrote the manuscript, and all the authors contributed to reviewing and editing.

Competing interests

The authors declare that they have no conflict of interests.

Acknowledgements

The authors gratefully acknowledge the Japan International Cooperation Agency (JICA) and Japan Science and Technology Agency (JST) through the Science and Technology Research Partnership for Sustainable Development Program (SATREPS) for financially supporting the project Comprehensive Assessment and Conservation of Blue Carbon Ecosystems ad their Services in the Coral Triangle (BlueCARES). We thank Dr. Charissa Ferrera for providing language help. Finally, the authors thank the reviewers for their feedback and comments that helped improve the manuscript.

References

Ashall, L. M., Mulligan, R. P., van Proosdij, D., and Poirier, E.: Application and validation of a three-dimensional hydrodynamic model of a macrotidal salt marsh. Coastal Engineering, 114, 35–46. https://doi.org/10.1016/j.coastaleng.2016.04.005, 2016.

Azman, M. S., Sharma, S., Shaharudin, M. A. M., Hamzah, M. L., Adibah, S. N., Zakaria, R. M., and MacKenzie, R. A.: Stand structure, biomass and dynamics of naturally regenerated and restored mangroves in Malaysia. Forest Ecology and Management, 482, 118852. https://doi.org/10.1016/j.foreco.2020.118852, 2021.

Best, Ü. S., van der Wegen, M., Dijkstra, J., Reyns, J., van Prooijen, B. C., and Roelvink, D.: Wave attenuation potential, sediment properties and mangrove growth dynamics data over Guyana's intertidal mudflats: assessing the potential of mangrove restoration works. Earth System Science Data, 14(5), 2445–2462. https://doi.org/10.5194/essd-14-2445-2022, 2022.

Beudin, A., Kalra, T. S., Ganju, N. K., and Warner, J. C.: Development of a coupled wave-flow-vegetation interaction model. Computers & Geosciences, 100, 76–86. https://doi.org/10.1016/j.cageo.2016.12.010, 2017.

Boechat Albernaz, M., Roelofs, L., Pierik, H. J., and Kleinhans, M. G.: Natural levee evolution in vegetated fluvial-tidal environments. Earth surface processes and landforms, 45(15), 3824–3841. https://doi.org/10.1002/esp.5003, 2020.

Bouma, T. J., Van Duren, L. A., Temmerman, S., Claverie, T., Blanco-Garcia, A., Ysebaert, T., and Herman, P. M. J.: Spatial flow and sedimentation patterns within patches of epibenthic structures: Combining field, flume and modelling experiments. Continental Shelf Research, 27(8), 1020–1045. https://doi.org/10.1016/j.csr.2005.12.019, 2007.

Breda, A., Saco, P. M., Sandi, S. G., Saintilan, N., Riccardi, G., and Rodríguez, J. F.: Accretion, retreat and transgression of coastal wetlands experiencing sea-level rise. Hydrology and Earth System Sciences, 25(2), 769–786. https://doi.org/10.5194/hess-25-769-2021, 2021.

Brückner, M. Z., Schwarz, C., van Dijk, W. M., van Oorschot, M., Douma, H., and Kleinhans, M. G.: Salt marsh establishment and eco-engineering effects in dynamic estuaries determined by species growth and mortality. Journal of Geophysical Research: Earth Surface, 124(12), 2962–2986. https://doi.org/10.1029/2019JF005092, 2019.

Bryan, K. R., Nardin, W., Mullarney, J. C., and Fagherazzi, S.: The role of cross-shore tidal dynamics in controlling intertidal sediment exchange in mangroves in Cù Lao Dung, Vietnam. Continental Shelf Research, 147, 128–143. https://doi.org/10.1016/j.csr.2017.06.014, 2017.

Chen, Y., Li, Y., Cai, T., Thompson, C., and Li, Y.: A comparison of biohydrodynamic interaction within mangrove and saltmarsh boundaries. Earth Surface Processes and Landforms, 41(13), 1967–1979. https://doi.org/10.1002/esp.3964, 2016.

Chen, Y., Li, Y., Thompson, C., Wang, X., Cai, T., and Chang, Y.: Differential sediment trapping abilities of mangrove and saltmarsh vegetation in a subtropical estuary. Geomorphology, 318, 270–282. https://doi.org/10.1016/j.geomorph.2018.06.018, 2018.

Dai, W., Yang, B., Dong, Z., and Shaker, A.: A new method for 3D individual tree extraction using multispectral airborne LiDAR point clouds. ISPRS journal of photogrammetry and remote sensing, 144, 400–411. https://doi.org/10.1016/j.isprsjprs.2018.08.010, 2018.

Defina, A. and Bixio, A. C.: Mean flow and turbulence in vegetated open channel flow. Water Resources Research, 41(7). https://doi.org/10.1029/2004WR003475, 2005.

Fagherazzi, S., Kirwan, M. L., Mudd, S. M., Guntenspergen, G. R., Temmerman, S., D'Alpaos, A., van de Koppel, J., Rybczyk, J. M, Reyes, E., Craft, C., and Clough, J.: Numerical models of salt marsh evolution: Ecological, geomorphic, and climatic factors. Reviews of Geophysics, 50(1). https://doi.org/10.1029/2011RG000359, 2012.

Fagherazzi, S., Mariotti, G., Leonardi, N., Canestrelli, A., Nardin, W., and Kearney, W. S.: Salt marsh dynamics in a period of accelerated sea level rise. Journal of Geophysical Research: Earth Surface, 125, e2019JF005200. https://doi.org/10.1029/2019JF005200, 2020.

Friess, D. A., Rogers, K., Lovelock, C. E., Krauss, K. W., Hamilton, S. E., Lee, S. Y., Lucas, R., Primavera, J., Rajkaran, R., and Shi, S.: The state of the world's mangrove forests: past, present, and future. Annu. Rev. Environ. Resour, 44(1), 89–115. https://doi.org/10.1146/annurev-environ-101718-033302, 2019.

Furukawa, K., Wolanski, E., and Mueller, H.: Currents and sediment transport in mangrove forests. Estuarine, Coastal and Shelf Science, 44(3), 301–310. https://doi.org/10.1006/ecss.1996.0120, 1997.

Hamilton, S. E. and Casey, D.: Creation of a high spatio-temporal resolution global database of continuous mangrove forest cover for the 21st century (CGMFC-21). Global Ecology and Biogeography, 25(6), 729–738. https://doi.org/10.1111/geb.12449, 2016.

Horstman, E. M., Dohmen-Janssen, C. M., Bouma, T. J., and Hulscher, S. J.: Tidal-scale flow routing and sedimentation in mangrove forests: Combining field data and numerical modelling. Geomorphology, 228, 244–262. https://doi.org/10.1016/j.geomorph.2014.08.011, 2015.

Horstman, E., Dohmen-Janssen, M., and Hulscher, S. J. M. H.: Modeling tidal dynamics in a mangrove creek catchment in Delft3D. Coastal Dynamics Arcachon, France, 833–844, 24–28 June 2013.

Jucker, T., Caspersen, J., Chave, J., Antin, C., Barbier, N., Bongers, F., Dalponte, M., van Ewijk, K. Y., Forrester, D. I., Haeni, M., Higgins, S. I., Holdaway, R. J., Iida, Y., Lorimer, C., Marshall, P. L., Momo, S., Moncrieff, G. R., Ploton, P., Poorter, L., Rahman, K. A., Schlund, M., Sonké, B., Sterck, F. J., Trugman, A. T., Usoltsev, V. A., Vanderwel, M. C., Waldner, P., Wedeux, B. M. M., Wirth, C., Wöll, H., Woods, M., Xiang, W., Zimmermann, N. E., and Coomes, D. A.: Allometric equations for integrating remote sensing imagery into forest monitoring programmes. Global change biology, 23(1), 177–190. https://doi.org/10.1111/gcb.13388, 2017.

Kalra, T. S., Ganju, N. K., Aretxabaleta, A. L., Carr, J. A., Defne, Z., and Moriarty, J. M.: Modeling marsh dynamics using a 3-D coupled wave-flow-sediment model. Front. Mar. Sci. 8. doi: 10.3389/fmars.2021.740921, 2022.

Katul, G. G., Mahrt, L., Poggi, D., and Sanz, C.: One-and two-equation models for canopy turbulence. Boundary-layer meteorology, 113(1), 81–109. https://doi.org/10.1023/B:BOUN.0000037333.48760.e5, 2004.

King, A. T., Tinoco, R. O., and Cowen, E. A.: A k–ε turbulence model based on the scales of vertical shear and stem wakes valid for emergent and submerged vegetated flows. Journal of Fluid Mechanics, 701, 1–39. https://doi.org/10.1017/jfm.2012.113, 2012.

Kirwan, M. L., Temmerman, S., Skeehan, E. E., Guntenspergen, G. R., and Fagherazzi, S.: Overestimation of marsh vulnerability to sea level rise. Nature Climate Change, 6(3), 253–260. https://doi.org/10.1038/nclimate2909, 2016.

Krauss, K. W., Allen, J. A., and Cahoon, D. R.: Differential rates of vertical accretion and elevation change among aerial root types in Micronesian mangrove forests. Estuarine, Coastal and Shelf Science, 56(2), 251–259. https://doi.org/10.1016/S0272-7714(02)00184-1, 2003.

Krauss, K. W., McKee, K. L., Lovelock, C. E., Cahoon, D. R., Saintilan, N., Reef, R., and Chen, L.: How mangrove forests adjust to rising sea level. New Phytologist, 202(1), 19–34. https://doi.org/10.1111/nph.12605, 2014.

Le Minor, M., Zimmer, M., Helfer, V., Gillis, L. G., Huhn, K.: Flow and sediment dynamics around structures in mangrove ecosystems—a modeling perspective, in: Dynamic Sedimentary Environments of Mangrove Coasts, edited by Sidik, F. and Friess, D. A., Elsevier, 83–120, https://doi.org/10.1016/B978-0-12-816437-2.00012-4, 2021.

Li, C. W. and Busari, A. O.: Hybrid modeling of flows over submerged prismatic vegetation with different areal densities. Engineering Applications of Computational Fluid Mechanics, 13(1), 493–505. https://doi.org/10.1080/19942060.2019.1610501, 2019.

Liu, C., Shan, Y., and Nepf, H.: Impact of stem size on turbulence and sediment resuspension under unidirectional flow. Water Resources Research, 57(3), e2020WR028620. https://doi.org/10.1029/2020WR028620, 2021.

Liu, D., Diplas, P., Fairbanks, J. D., and Hodges, C. C.: An experimental study of flow through rigid vegetation, J. Geophys. Res., 113, F04015, doi:10.1029/2008JF001042, 2008.

Liu, Z., Chen, Y., Wu, Y., Wang, W., and Li, L.: Simulation of exchange flow between open water and floating vegetation using a modified RNG *k-ε* turbulence model. Environ Fluid Mech 17, 355–372. https://doi.org/10.1007/s10652-016-9489-5, 2017.

Lokhorst, I. R., Braat, L., Leuven, J. R., Baar, A. W., Van Oorschot, M., Selaković, S., and Kleinhans, M. G.: Morphological effects of vegetation on the tidal–fluvial transition in Holocene estuaries. Earth Surface Dynamics, 6(4), 883–901. https://doi.org/10.5194/esurf-6-883-2018, 2018.

López, F. and García, M. H.: Mean flow and turbulence structure of open-channel flow through non-emergent vegetation. Journal of Hydraulic Engineering, 127(5), 392–402. https://doi.org/10.1061/(ASCE)0733-9429(2001)127:5(392), 2001.

Lovelock, C. E., Cahoon, D. R., Friess, D. A., Guntenspergen, G. R., Krauss, K. W., Reef, R., Rogers, K., Saunders, M. L., Sidik, F., Swales, A., Saintilan, N., Thuyen, L. X, and Triet, T.: The vulnerability of Indo-Pacific mangrove forests to sea-level rise. Nature, 526(7574), 559–563. https://doi.org/10.1038/nature15538, 2015.

Mariotti, G. and Canestrelli, A.: Long-term morphodynamics of muddy backbarrier basins: Fill in or empty out?. Water Resources Research, 53(8), 7029–7054. https://doi.org/10.1002/2017WR020461, 2017.

Mariotti, G. and Fagherazzi, S.: A numerical model for the coupled long-term evolution of salt marshes and tidal flats. Journal of Geophysical Research: Earth Surface, 115(F1). https://doi.org/10.1029/2009JF001326, 2010.

Marsooli, R., Orton, P. M., Georgas, N., and Blumberg, A. F.: Three-dimensional hydrodynamic modeling of coastal flood mitigation by wetlands. Coastal Engineering, 111, 83–94. https://doi.org/10.1016/j.coastaleng.2016.01.012, 2016.

Maza, M., Adler, K., Ramos, D., Garcia, A. M., and Nepf, H.: Velocity and drag evolution from the leading edge of a model mangrove forest. Journal of Geophysical Research: Oceans, 122(11), 9144–9159. https://doi.org/10.1002/2017JC012945, 2017.

Menéndez, P., Losada, I. J., Torres-Ortega, S., Narayan, S., and Beck, M. W.: The global flood protection benefits of mangroves. Scientific reports, 10(1), 1–11. https://doi.org/10.1038/s41598-020-61136-6, 2020.

Mori, N., Chang, C. W., Inoue, T., Akaji, Y., Hinokidani, K., Baba, S., Takagi, M., Mori, S., Koike, H., Miyauchi, M., Suganuma, R., Sabunas, A., Miyashita, T., and Shimura, T.: Parameterization of mangrove root structure of *Rhizophora stylosa* in coastal hydrodynamic model. Frontiers in Built Environment, 7, 782219. https://doi.org/10.3389/fbuil.2021.782219, 2022.

Mudd, S. M., D'Alpaos, A., and Morris, J. T.: How does vegetation affect sedimentation on tidal marshes? Investigating particle capture and hydrodynamic controls on biologically mediated sedimentation. Journal of Geophysical Research: Earth Surface, 115(F3). https://doi.org/10.1029/2009JF001566, 2010.

Mullarney, J. C., Henderson, S. M., Reyns, J. A., Norris, B. K., and Bryan, K. R.: Spatially varying drag within a wave-exposed mangrove forest and on the adjacent tidal flat. Continental Shelf Research, 147, 102-113. https://doi.org/10.1016/j.csr.2017.06.019, 2017.

Nardin, W. and Edmonds, D. A.: Optimum vegetation height and density for inorganic sedimentation in deltaic marshes. Nature Geoscience, 7(10), 722–726. https://doi.org/10.1038/ngeo2233, 2014.

Nardin, W., Edmonds, D. A., and Fagherazzi, S.: Influence of vegetation on spatial patterns of sediment deposition in deltaic islands during flood. Advances in Water Resources, 93, 236–248. https://doi.org/10.1016/j.advwatres.2016.01.001, 2016.

Nepf, H. M.: Drag, turbulence, and diffusion in flow through emergent vegetation. Water resources research, 35(2), 479–489. https://doi.org/10.1029/1998WR900069, 1999.

Nepf, H. M.: Flow and transport in regions with aquatic vegetation. Annual review of fluid mechanics, 44, 123–142. https://doi.org/10.1146/annurev-fluid-120710-101048, 2012.

Ohira, W., Honda, K., Nagai, M., and Ratanasuwan, A.: Mangrove stilt root morphology modeling for estimating hydraulic drag in tsunami inundation simulation. Trees, 27(1), 141–148. https://doi.org/10.1007/s00468-012-0782-8, 2013.

Otero, V., Van De Kerchove, R., Satyanarayana, B., Martínez-Espinosa, C., Fisol, M. A. B., Ibrahim, M. R. B., Sulong, I., Mohd-Lokman, H., Lucas, R., and Dahdouh-Guebas, F.: Managing mangrove forests from the sky: Forest inventory using field data and Unmanned Aerial Vehicle (UAV) imagery in the Matang Mangrove Forest Reserve, peninsular Malaysia. Forest Ecology and Management, 411, 35–45. https://doi.org/10.1016/j.foreco.2017.12.049, 2018.

Rodríguez, J. F., Saco, P. M., Sandi, S., Saintilan, N., and Riccardi, G.: Potential increase in coastal wetland vulnerability to sea-level rise suggested by considering hydrodynamic attenuation effects. Nature communications, 8(1), 1–12. https://doi.org/10.1038/ncomms16094, 2017.

Shan, Y., Liu, C., and Nepf, H.: Comparison of drag and velocity in model mangrove forests with random and in-line tree distributions. Journal of Hydrology, 568, 735–746. https://doi.org/10.1016/j.jhydrol.2018.10.077, 2019.

Shchepetkin, A. F. and McWilliams, J. C.: The regional oceanic modeling system (ROMS): a split-explicit, free-surface, topography-following-coordinate oceanic model. Ocean modelling, 9(4), 347–404. https://doi.org/10.1016/j.ocemod.2004.08.002, 2005.

Simard, M., Fatoyinbo, L., Smetanka, C., Rivera-Monroy, V. H., Castañeda-Moya, E., Thomas, N., and Van der Stocken, T.: Mangrove canopy height globally related to precipitation, temperature and cyclone frequency. Nature Geoscience, 12(1), 40–45. https://doi.org/10.1038/s41561-018-0279-1, 2019.

Suwa, R., Rollon, R., Sharma, S., Yoshikai, M., Albano, G. M. G., Ono, K., Adi, N. S., Ati, R. N. A., Kusumaningtyas, M. A., Kepel, T. L., Maliao, R. J., Primavera-Tirol, Y. H., Blanco, A. C., and Nadaoka, K.: Mangrove biomass estimation using canopy height and wood density in the South East and East Asian regions. Estur. Coast. Shelf S., 248, 106937, 2021.

Tanino, Y. and Nepf, H. M.: Lateral dispersion in random cylinder arrays at high Reynolds number. Journal of Fluid Mechanics, 600, 339–371. https://doi.org/10.1017/S0022112008000505, 2008.

Temmerman, S., Bouma, T. J., Govers, G., Wang, Z. B., De Vries, M. B., and Herman, P. M. J.: Impact of vegetation on flow routing and sedimentation patterns: Three-dimensional modeling for a tidal marsh. Journal of Geophysical Research: Earth Surface, 110(F4). https://doi.org/10.1029/2005JF000301, 2005.

Tinoco, R. O. and Coco, G.: A laboratory study on sediment resuspension within arrays of rigid cylinders. Advances in Water Resources, 92, 1–9. https://doi.org/10.1016/j.advwatres.2016.04.003, 2016.

Umlauf, L. and Burchard, H.: A generic length-scale equation for geophysical turbulence models. Journal of Marine Research, 61(2), 235–265. https://doi.org/10.1357/002224003322005087, 2003.

van Maanen, B., Coco, G., and Bryan, K. R.: On the ecogeomorphological feedbacks that control tidal channel network evolution in a sandy mangrove setting. Proceedings of the Royal Society A: Mathematical, Physical and Engineering Sciences, 471(2180), 20150115. https://doi.org/10.1098/rspa.2015.0115, 2015.

Warner, J. C., Armstrong, B., He, R., and Zambon, J. B.: Development of a coupled ocean–atmosphere–wave–sediment transport (COAWST) modeling system. Ocean modelling, 35(3), 230–244. https://doi.org/10.1016/j.ocemod.2010.07.010, 2010.

Warner, J. C., Sherwood, C. R., Arango, H. G., and Signell, R. P.: Performance of four turbulence closure models implemented using a generic length scale method. Ocean Modelling, 8(1-2), 81–113. https://doi.org/10.1016/j.ocemod.2003.12.003, 2005.

Weisscher, S. A. H., Van den Hoven, K., Pierik, H. J., and Kleinhans, M.: Building and raising land: mud and vegetation effects in infilling estuaries. Journal of Geophysical Research: Earth Surface, 127(1). https://doi.org/10.1029/2021JF006298, 2022.

Willemsen, P. W. J. M., Horstman, E. M., Borsje, B. W., Friess, D. A., and Dohmen-Janssen, C. M.: Sensitivity of the sediment trapping capacity of an estuarine mangrove forest. Geomorphology, 273, 189–201. https://doi.org/10.1016/j.geomorph.2016.07.038, 2016.

Willemsen, P. W. J. M., Smits, B. P., Borsje, B. W., Herman, P. M. J., Dijkstra, J. T., Bouma, T. J., and Hulscher, S. J. M. H.: Modeling decadal salt marsh development: variability of the salt marsh edge under influence of waves and sediment availability. Water resources research, 58(1), e2020WR028962. https://doi.org/10.1029/2020WR028962, 2022.

Xie, D., Schwarz, C., Brückner, M. Z., Kleinhans, M. G., Urrego, D. H., Zhou, Z., and Van Maanen, B.: Mangrove diversity loss under sea-level rise triggered by bio-morphodynamic feedbacks and anthropogenic pressures. Environmental Research Letters, 15(11), 114033. https://doi.org/10.1088/1748-9326/abc122, 2020.

Xu, Y., Esposito, C. R., Beltrán-Burgos, M., and Nepf, H. M.: Competing effects of vegetation density on sedimentation in deltaic marshes. Nature communications, 13(1), 1–10. https://doi.org/10.1038/s41467-022-32270-8, 2022.

Xu, Y. and Nepf, H.: Measured and predicted turbulent kinetic energy in flow through emergent vegetation with real plant morphology. Water Resources Research, 56(12), e2020WR027892. https://doi.org/10.1029/2020WR027892, 2020.

Xu, Y. and Nepf, H.: Suspended sediment concentration profile in a *Typha latifolia* canopy. Water Resources Research, 57(9), e2021WR029902. https://doi.org/10.1029/2021WR029902, 2021.

Yang, J. Q. and Nepf, H. M.: A turbulence-based bed-load transport model for bare and vegetated channels. Geophysical Research Letters, 45(19), 10–428. https://doi.org/10.1029/2018GL079319, 2018.

Yoshikai, M: MasayaYoshikai/COAWST_mangrove_rh: COAWST_rh (v1.0), Zenodo [code], https://zenodo.org/record/7353835#.Y4BZoZrP1D9, 2022.

Yoshikai, M., Nakamura, T., Suwa, R., Argamosa, R., Okamoto, T., Rollon, R., Basina, R., Primavera-Tirol, Y. H., Blanco, A. C., Adi, N. S., and Nadaoka, K.: Scaling relations and substrate conditions controlling the complexity of Rhizophora prop root system. Estur. Coast. Shelf S., 248, 107014, 2021.

Yoshikai, M., Nakamura, T., Bautista, D. M., Herrera, E. C., Baloloy, A., Suwa, R., Basina, R., Primavera-Tirol, Y. H., Blanco, A.C., and Nadaoka, K.: Field measurement and prediction of drag in a planted *Rhizophora* mangrove forest. Journal of Geophysical Research: Oceans, 127, e2021JC018320. https://doi.org/10.1029/2021JC018320, 2022a.

Yoshikai, M., Nakamura, T., Suwa, R., Sharma, S., Rollon, R., Yasuoka, J., Egawa, R., and Nadaoka, K.: Predicting mangrove forest dynamics across a soil salinity gradient using an individual-based vegetation model linked with plant hydraulics. Biogeosciences, 19(6), 1813–1832. https://doi.org/10.5194/bg-19-1813-2022, 2022b.

Zhang, K., Liu, H., Li, Y., Xu, H., Shen, J., Rhome, J., and Smith III, T. J.: The role of mangroves in attenuating storm surges. Estuarine, Coastal and Shelf Science, 102, 11–23. https://doi.org/10.1016/j.ecss.2012.02.021, 2012.

Zhang, X., Chua, V. P., and Cheong, H. F.: Hydrodynamics in mangrove prop roots and their physical properties. Journal of hydro-environment research, 9(2), 281–294. https://doi.org/10.1016/j.jher.2014.07.010, 2015.

Zhang, Y., Svyatsky, D., Rowland, J. C., Moulton, J. D., Cao, Z., Wolfram, P. J., Xu, C., and Pasqualini, D. (2022). Impact of coastal marsh eco-geomorphologic change on saltwater intrusion under future sea level rise. Water Resources Research, e2021WR030333. https://doi.org/10.1029/2021WR030333.

Zhu, Q., Wiberg, P. L., and Reidenbach, M. A.: Quantifying Seasonal Seagrass Effects on Flow and Sediment Dynamics in a Back-Barrier Bay. Journal of Geophysical Research: Oceans, 126(2), e2020JC016547. https://doi.org/10.1029/2020JC016547, 2021.